Cell Reports

Article

Human monoclonal antibodies that target the SFTSV glycoprotein Gn head from four neutralizing epitope groups

Graphical abstract

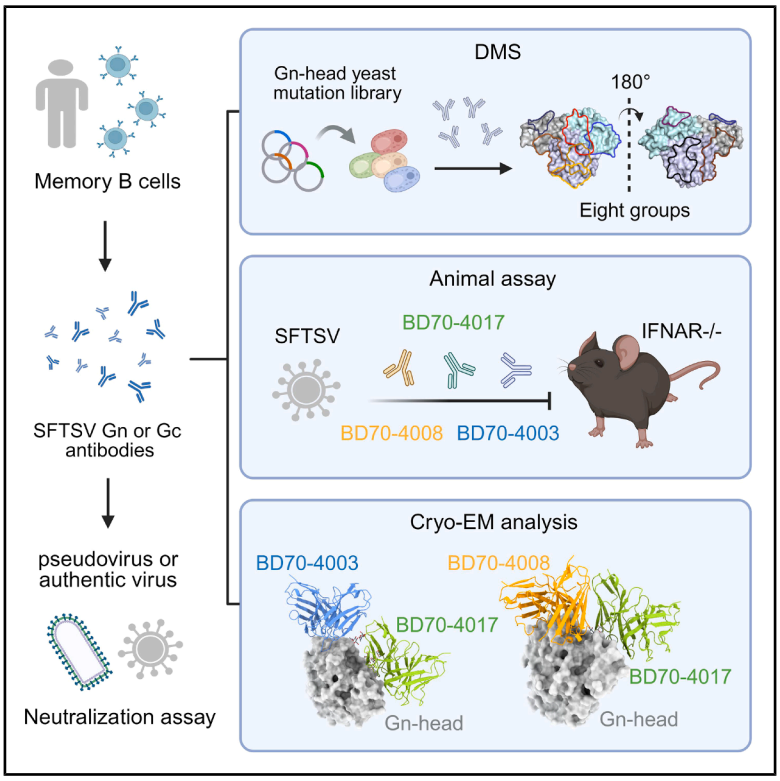

Highlights

- Human mAbs from survivors broadly neutralize SFTSV variants
- DMS maps Gn-head mAbs to eight distinct epitope groups
- Cryo-EM structures confirm DMS-inferred epitopes with precision
- Two distinct-epitope Gn mAbs protect mice from SFTSV infection

Authors

Qianran Wang, Hao Li, Fanchong Jian, ..., Liuluan Zhu, Wei Liu, Yunlong Cao

Correspondence

zhuliuluan@ccmu.edu.cn (L.Z.), liuwei@bmi.ac.cn (W.L.), yunlongcao@pku.edu.cn (Y.C.)

In brief

Wang et al. report that Gn-specific mAbs from SFTS survivors exhibit broad and potent neutralization, with two providing complete protection in a lethal mouse model. This work maps the Gn antigenic landscape and establishes a deep mutational scanning platform coupled with structural validation for bunyavirus antibody discovery.

Wang et al., 2026, Cell Reports *45*, 117248
April 28, 2026
https://doi.org/10.1016/j.celrep.2026.117248

CellPress

Cell Reports

CellPress
OPEN ACCESS

Article

Human monoclonal antibodies that target the SFTSV glycoprotein Gn head from four neutralizing epitope groups

Qianran Wang,[1,8] Hao Li,[2,8] Fanchong Jian,[3] Aoxiang Han,[2] Yuanni Liu,[4] Jingyi Liu,[1,5] Yuanling Yu,[1] Jing Wang,[1] Lingling Yu,[1] Yanxia Wang,[1] Haiyan Sun,[1] Miaomiao Ma,[1] Fei Shao,[1] Liuluan Zhu,[6,*] Wei Liu,[2,*] and Yunlong Cao[1,3,7,9,*]

[1]Changping Laboratory, Beijing, P.R. China
[2]State Key Laboratory of Pathogen and Biosecurity, Academy of Military Medical Sciences, Beijing, P.R. China
[3]Biomedical Pioneering Innovation Center (BIOPIC), School of Life Sciences, Peking University, Beijing, China
[4]Department of Infectious Diseases, Yantai Qishan Hospital, Yantai, P.R. China
[5]College of Future Technology, Peking University, Beijing, P.R. China
[6]Beijing Key Laboratory of Viral Infectious Diseases, Beijing Ditan Hospital, Capital Medical University, Beijing, P.R. China
[7]Peking-Tsinghua Center for Life Sciences, Peking University, Beijing, P.R. China
[8]These authors contributed equally
[9]Lead contact
*Correspondence: zhuliuluan@ccmu.edu.cn (L.Z.), liuwei@bmi.ac.cn (W.L.), yunlongcao@pku.edu.cn (Y.C.)
https://doi.org/10.1016/j.celrep.2026.117248

SUMMARY

Severe fever with thrombocytopenia syndrome virus (SFTSV) is a lethal bunyavirus lacking approved countermeasures. From SFTS survivors, we isolate 84 human monoclonal antibodies (mAbs) against the viral glycoproteins Gn and Gc. Gn-specific mAbs demonstrate superior neutralization breadth and potency compared to the restricted neutralizing activity observed with Gc. Using a high-throughput yeast display deep mutational scanning (DMS) platform, we classify Gn-head mAbs into eight epitope groups, among which four groups (IA, ID, IIIA, and IIIB) confer neutralization. Notably, mAbs BD70-4003 (group IA) and BD70-4017 (group IIIA) exhibit broad neutralization and provide 100% protection in a lethal mouse model. Cryo-electron microscopy (cryo-EM) structural analysis of these mAbs in complex with the Gn head reveals their binding interfaces, directly validating the epitope residues identified by DMS. Our study delineates the antigenic landscape of SFTSV Gn, identifies potent therapeutic candidates, and establishes DMS coupled with structural validation as a powerful framework for antibody discovery against bunyaviruses.

INTRODUCTION

Severe fever with thrombocytopenia syndrome virus (SFTSV), or *Bandavirus dabieense*, is an emerging tick-borne phlebovirus first identified in China in 2009 and that has since been reported across East and Southeast Asia, including Japan, South Korea, Vietnam, Pakistan, and Thailand.[1–3] Clinical manifestations range from fever, thrombocytopenia, and leukopenia to multi-organ dysfunction, with a subset of patients developing hemorrhagic symptoms and organ failure. The case fatality rate (CFR) is approximately 16.2% (95% confidence interval [CI]: 14.6–17.8) among confirmed cases.[4–6] The principal vector, the Asian longhorned tick, has recently been detected in North America, Russia, and Australia, raising concerns regarding geographic expansion and the increasing risk of human-to-human transmission.[7–9] Despite its designation by the World Health Organization as a priority pathogen requiring urgent countermeasures, no licensed vaccines or effective antiviral drugs are currently available.

The tripartite SFTSV genome encodes a glycoprotein precursor on the M segment, which is cleaved into Gn and Gc subunits that mediate receptor binding and membrane fusion during viral entry.[10,11] These glycoproteins are the primary mediators of viral entry; Gn is generally implicated in initial receptor attachment, while Gc facilitates the low-pH-dependent fusion of the viral and endosomal membranes. These Gn/Gc heterodimers organize into higher-order hexon and penton structures, creating a dense and ordered lattice that covers the viral envelope.[12]

Recent structural biology breakthroughs have suggested the Gn glycoprotein as an immunodominant target for neutralizing monoclonal antibodies (mAbs).[12] The Gn ectodomain consists of a globular head and a stem region. The Gn head (residues 20–340) is further subdivided into three distinct structural domains: domains I, II, and III. Domain I is characterized by high surface exposure and is believed to harbor the critical interfaces for host receptor engagement. Domain II acts as a β-connector structure, while domain III forms a structural "cap" that partially shields the fusion loop of the Gc subunit, thereby regulating the timing of membrane fusion. The preservation of these domains across diverse SFTSV clades makes them attractive targets for the development of universal therapeutics and vaccine antigens.

Multiple mAbs against Gn have been described, but their epitopes, potency, and breadth vary significantly.[13–19] A systematic evaluation is essential to delineate the precise relationship between Gn-directed antibody epitopes and neutralization potency, both *in vitro* and *in vivo*, to inform the development of therapeutics and vaccines. Deep mutational scanning (DMS) technology enables epitope mapping with significantly higher efficiency and resolution than traditional binning techniques.[20,21] We previously developed a high-throughput epitope mapping platform based on DMS to study SARS-CoV-2, establishing a pipeline to isolate large panels of mAbs and simultaneously identify their precise binding epitopes.[22–27] Here, we applied this technology to SFTSV to elucidate the intrinsic relationship between antigenic epitopes and functional antibody profiles.

We report the isolation and epitope classification of human mAbs from SFTSV convalescents. We assessed binding and neutralization using enzyme-linked immunosorbent assays (ELISAs), pseudovirus assays, and authentic virus neutralization assays. Using a novel yeast DMS approach adapted for bunyaviruses, we classified Gn-head mAbs into eight epitope groups (IA–ID, IIA, IIB, IIIA, and IIIB). Four groups (IA, ID, IIIA, and IIIB) demonstrated neutralizing activity. Two antibodies in particular—BD70-4003 (IA) and BD70-4017 (IIIA)—exhibited broad neutralization and provided 100% protection in mice, making them promising drug candidates. Cryo-electron microscopy (cryo-EM) structural analyses of three mAbs (BD70-4003, BD70-4008, and BD70-4017) defined the molecular basis of recognition and verified the accuracy of our DMS system. Our results elucidate the overall epitope distribution of the SFTSV Gn-head domain and identify highly potent neutralizing antibodies targeting distinct epitopes, providing theoretical guidance for future therapeutic and vaccine design.

RESULTS

Isolation of mAbs from SFTS convalescents

We collected whole-blood samples from 12 SFTSV survivors who had been infected for more than 1 year (Table S1). Serum samples were analyzed for viral Gn/Gc-specific IgG titers and for neutralizing activities against SFTSV pseudovirus. The results showed that the Gn or Gc reactive antibody remained at high levels in these serum samples (Figure 1A), and the serum exhibited high neutralizing activity against six pseudovirus strains (Figure 1B). This is consistent with previous reports that SFTSV glycoproteins induce long-lasting antibodies and also suggests the possibility of potentially broadly neutralizing antibodies.[28,29]

To isolate mAbs, we purified antigen-specific memory B cells from peripheral blood mononuclear cells (PBMCs) using fluorescence-activated cell sorting (FACS). From the PBMCs, $CD19^+$ IgM^- $CD27^+$ memory B cells were stained simultaneously with HB29 Gn and Gc glycoproteins, and cells positive for either antigen were sorted as antigen-specific B cells (Figure S1A). To distinguish Gn- and Gc-specific responses during sequencing, each antigen was labeled with a unique DNA barcode. In total, we retrieved 1,316 paired heavy-light-chain antigen-specific antibody sequences using high-throughput single-cell V(D)J sequencing.

A subset of antibody sequences was randomly selected for expression and further functional characterization. In total, we expressed 54 Gn-specific and 44 Gc-specific IgG1 antibodies *in vitro*. ELISA confirmed binding activity in 49/54 (90.7%) of the Gn group and 35/44 (79.5%) of the Gc group (Table S2). ELISA-positive Gn (n = 49) and Gc (n = 35) mAbs were subsequently subjected to neutralization assays.

In the neutralization assay, we employed 9 vesicular stomatitis virus (VSV)-based pseudovirus strains representing six major SFTSV genotypes (A–F) (Tables S3, S4, S5, and S6).[30–32] These strains include HB29 (genotype D), HBMC16 (genotype D), WCH (genotype A), HN13 (genotype A), HN20 (genotype F), G/K/2012 (genotype F), SD4 (genotype E), SPL030A (genotype B), and AHL (genotype C). The results show that mAbs against Gn exhibited more potent neutralization effects against the pseudovirus than those against Gc, which is consistent with previous reports that neutralizing antibodies against SFTSV primarily target the Gn antigen (Figures 1C and 1D).[14,33–35] This observation was further validated in authentic virus neutralization assays, where eleven selected Gn-specific pseudovirus neutralizing mAbs—but zero Gc-specific mAbs—showed greater than 50% inhibition against the HBMC strain at 0.25 μg/mL (Figure S1B). Based on these results, we confirm that Gn is the immunodominant antigen target for SFTSV neutralizing antibodies.

Epitope mapping via DMS

Defining antibody epitopes is essential for understanding neutralization mechanisms and for identifying functionally important regions on viral antigens that can be targeted for therapeutic or vaccine development. To provide a high-resolution epitope map of the Gn antigenic surface, a comprehensive DMS platform was implemented.[21,36–38] A yeast display library of the HB29 Gn-head domain (residues 20–340) was constructed, incorporating nearly all possible amino acid substitutions at each position. By subjecting this library to antibody selection and high-throughput sequencing of escape variants, critical binding residues were identified for 44 newly isolated human Gn mAbs and several benchmark control antibodies. Specifically, we performed negative-selection FACS to isolate yeast cells that failed to bind specific antibodies, followed by sequencing to identify critical escape mutants. Unsupervised clustering of the resulting escape profiles partitioned the Gn head into eight distinct epitope groups, providing a systematic framework for understanding antibody function.

The eight epitope groups (IA–ID, IIA, IIB, IIIA, and IIIB) demonstrate a diverse distribution across the Gn-head structure (Figures 2A–2C and S2). Groups IA, IC, and ID are localized to domain I. Group IA, represented by elite neutralizing mAbs such as BD70-4003, targets a surface-exposed region involving residues D159, G161, S163-S164, and L166. Groups IC (e.g., control antibody SF5[39]) and ID (e.g., control antibody 40C10[16]) target distinct sites on the opposite faces of domain I. Domain II is recognized by groups IIA and IIB, which include antibodies such as N1D10 and B1G11.[15] No convergent V(D)J gene usage was observed within mAbs targeting domains I and II (Figure 2D). Despite high binding scores, antibodies targeting domain II often exhibit poor neutralizing activity, most likely due to the domain's

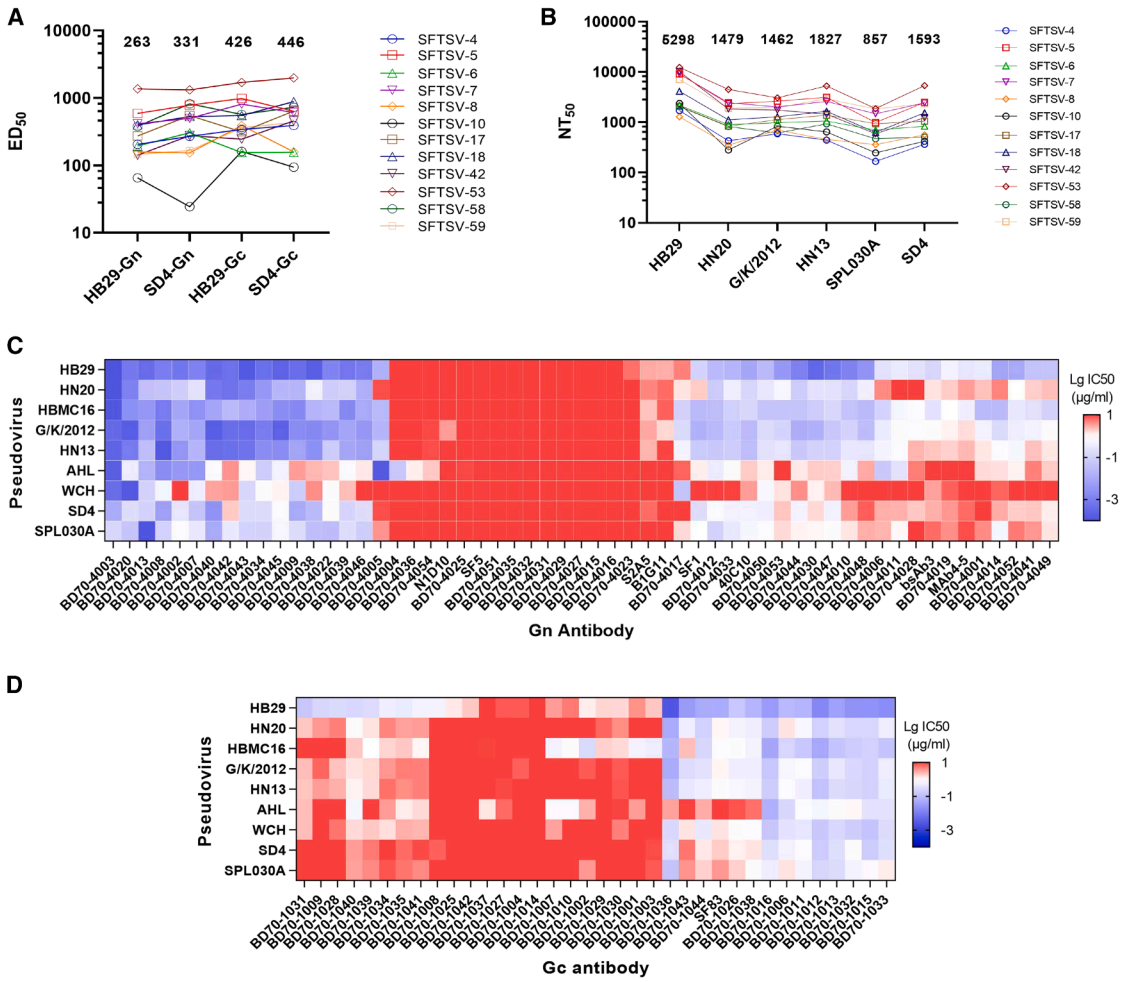

Figure 1. Identification of broad neutralizing antibodies from SFTSV-infected convalescents

(A) The median effective dose (ED_{50}) of plasma from SFTSV-infected convalescents was determined by ELISA. The average value of each group was marked.

(B) The half-maximal neutralization titer (NT_{50}) of plasma against VSV-based SFTSV pseudoviruses.

(C and D) Neutralizing median inhibition concentration (IC_{50}; μg/mL) of SFTSV Gn (C) or Gc (D) antibodies using VSV-based pseudoviruses. Neutralization assays were conducted in at least two biological replicates.

See also Figure S1 and Tables S1, S2, S3, S4, and S5.

less accessible orientation on the mature virion (Figures 2E and 2F).

Group III antibodies are subdivided into IIIA and IIIB and target domain III. Group IIIA antibodies, such as BD70-4017, interact with a cluster of residues including Q73–R74, G264–P265, and E271. Group IIIB antibodies, including the well-characterized MAb4-5,[13] focus on an epitope involving residues E271, G282, C287, K288, and C292. Notably, VDJ-encoding gene analysis of group IIIB mAbs showed frequent genes involving IGHV5-51 (Figure 2D). Importantly, comparative analysis reveals that the most potent neutralizing activity is concentrated in groups IA and IIIA, followed by IIIB and ID, whereas IC, IIA, and IIB are largely non-neutralizing. This trend was also consistent across another eight SFTSV pseudovirus strains, with the most potent neutralization again observed in the IA and IIIA antibody groups, highlighting the functional dominance of the IA and IIIA epitopes (Figure S3).

To validate the accuracy of our DMS platform, we compared our results with previously published crystal or cryo-EM structures. It has been reported that the interface between the Gn head and MAb4-5 (IIIB) was located on sites S251–F256, K275–G278, and M284–H294 by crystal structure analysis,[13] which was consistent with the key amino acids (C287–K288 and C292) we have screened (Figures 2B and 2C). For domain I antibodies SF5 (IC) and 40C10 (ID), DMS identified key residues S81–A85, S123–G126, and R171 for SF5 and H64–S65, K111–K113, and G142 for 40C10 (Figures 2B and 2C). Actually, SF5 (IC) bound to sites R74–S90, G121–G126, and T150–R171,[39] while 40C10 (ID) bound to sites R62–Q66, D102, K111–S115, and C156.[16] Except for site G142, which was close to S65, all sites in this study were consistent with their complex structures. Results of mAbs against domain II were also relatively accurate. According to Ren et al.'s study,[15] N1D10 (IIA) and B1G11 (IIB) mainly bound to sites E114–G121, G218–D226,

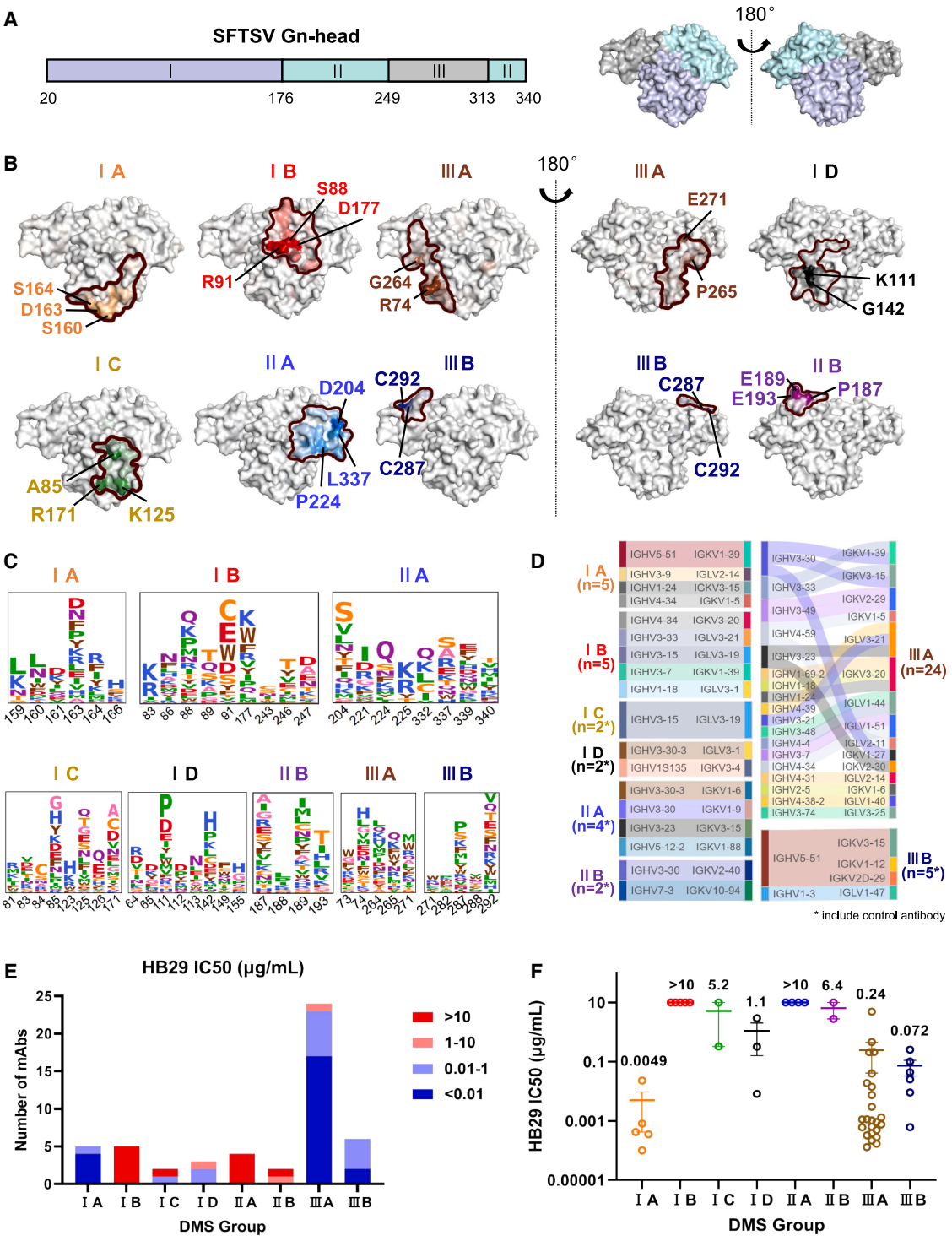

Figure 2. Epitope analysis of all Gn antibodies by yeast DMS

(A) Structural schematic of SFTSV Gn head. The left image illustrates the delineation of the three domains, colored in blue-white (I), pale cyan (II), and gray (III), respectively; the corresponding structural schematic is shown in the right image (PDB: 5Y10).

(B) Structural projections and key epitope annotations of the eight DMS groups with different colors. The region outlined by the curved line corresponds to the epitope of each respective group. In the structural projection, amino acid residues with higher DMS scores are displayed in darker colors.

(C) Average escape scores of antibodies in eight groups. Colors are assigned according to the type of amino acids, and the heights of the letters in the logo plot indicate escape scores. Residues are numbered based on Gn-head numbering.

(legend continued on next page)

and V339–N340 and P185–E193 and T321–V323, respectively, which also include the sites of our DMS results (Figures 2B and 2C). These correlations confirm that the yeast-based DMS library effectively captures the functional epitopes of SFTSV glycoproteins, providing a reliable alternative to high-throughput epitope determination for structural mapping.

Protective effect of Gn mAbs *in vitro* and *in vivo*

Previous pseudovirus and authentic virus neutralization screenings identified six Gn antibodies (BD70-4003, BD70-4008, BD70-4009, BD70-4013, BD70-4017, and BD70-4022) with broad inhibitory effects (Table S3). These elite candidates were also found to have undergone extensive affinity maturation, as evidenced by high somatic hypermutation (SHM) rates and binding affinities (Table S7; Figure S4). Notably, the binding affinities of BD70-4008 and BD70-4003 against Gn have reached the low picomolar range.

A focus reduction neutralization test (FRNT) was performed to further validate the neutralization capacity of these elite mAbs (Figure 3A).[18] All 6 Gn mAbs demonstrated potent neutralization *in vitro* with low $FRNT_{50}$ values (Figure 3B). Interestingly, although BD70-4017 showed relatively modest neutralization in the pseudovirus system compared to its peers, its performance against authentic SFTSV strains was dramatically enhanced, illustrating that pseudotype assays may not fully recapitulate the inhibitory potential of certain epitopes.

To evaluate the prophylactic and therapeutic efficacy of the 6 mAb candidates against SFTSV *in vivo*, *IFNAR1*$^{-/-}$ mice were challenged with SFTSV before or after treatment with the mAb. In prophylactic and therapeutic groups, 5 mg/kg antibody was given to the mice via intraperitoneal (i.p.) injection 1 day pre-infection or 1 day post-infection (dpi), respectively (Figures 3C and 3F). A vehicle group of mice that received a human IgG1 isotype control antibody was also included. Each group consisted of five or six mice. The body weight of each mouse in each group was monitored and recorded daily. Serum samples were collected from all mice on 3 dpi, with an additional collection performed for the therapeutic group on 5 dpi. Livers, spleens, and lungs were collected for viral load analyses via RT-qPCR.

In the prophylactic treatment group, most mice died between 5 and 6 dpi without mAb injection and exhibited significantly higher viral RNA copies in serum samples (Figures 3D and 3E). BD70-4003 (IA), BD70-4008 (IIIA), and BD70-4017 (IIIA) protected 100% of mice from SFTSV infection, while one mouse died on day 7 or 10 in the groups treated with BD70-4009 (IIIA), BD70-4013 (IA), and BD70-4022 (IIIA) (Figure 3D). Viral copy numbers in the serum of mice treated with BD70-4003, BD70-4008, or BD70-4017 were below the detection limit, indicating that these three antibodies exhibited superior efficacy in promoting viral clearance (Figure 3E).

In the therapeutic treatment group, BD70-4003 (IA) and BD70-4017 (IIIA) protected 100% of mice from SFTSV challenge (Figure 3G), and extremely low viral copy numbers were detected in serum samples collected on both 3 and 5 dpi (Figures 3H and 3I). The remaining four antibodies conferred weaker protective effects, with varying numbers of deaths occurring within their respective treatment groups. We also analyzed tissue samples collected on 5 dpi. Viral copy numbers in spleens, livers, and lungs from the BD70-4003 and BD70-4017 treatment groups were reduced by 3–4 log values compared to the vehicle group (Figures 3J–3L). All these results suggested that administration of either BD70-4003 (IA) or BD70-4017 (IIIA) exhibited significant therapeutic effects. The *in vivo* experimental results further validated our preliminary *in vitro* antibody screening strategy, demonstrating that antibodies targeting epitopes IA and IIIA hold the greatest potential for development as therapeutic antibodies.

Structural analyses of Gn-Ab complexes

To gain deeper insights into the molecular mechanisms underlying the distinct neutralizing activities of different antibodies, we selected 3 mAbs (BD70-4003, BD70-4008, and BD70-4017) for structural analysis. Among them, BD70-4003 and BD70-4008 exhibited competitive binding to Gn protein. Consequently, except for the Gn-head/BD70-4003 Fab and Gn-head/BD70-4008 Fab, we also designed 2 combinations of antibodies to form complexes with the Gn head for structural analysis, thereby increasing the complex size to facilitate structural determination. The Gn head/BD70-4003 Fab and Gn head/BD70-4008 Fab were detected by cryo-EM (Table S8), with their structure ultimately resolved at reported global resolution with 2.85 and 2.97 Å, respectively (Figures S5A and S5B). Two complexes, Gn head/BD70-4003 Fab/BD70-4017 Fab and Gn head/BD70-4008 Fab/BD70-4017 Fab, were also resolved with 2.69 Å resolution (Figures S5C and S5D).

The complex structure of the BD70-4003 Fab bound to the Gn head revealed a large interaction interface primarily located on domain I. Key contact residues on Gn included S32, K34, Q68, Q73–R74, S145–K147, S158–G161, S163–S164, and L166–S169 (Figures 4A and 4B). The interaction is stabilized by 11 hydrogen bonds, with the heavy chain (specifically residues D55, E100, D101, D104, and Y105) contributing the majority of the bonding potential (Figure 4C). This epitope overlaps significantly with the identified binding sites for the host receptor C-C motif chemokine receptor 2 (CCR2).[40] Specifically, the proximity to residue D170, which is a critical determinant of SFTSV Gn binding to CCR2, indicates that BD70-4003 neutralizes the virus by competitively inhibiting receptor attachment.[41]

In contrast, BD70-4017 primarily targets domain III, engaging residues K260–T263, P265, S267–E270, and A273–C280 (Figures 4D and 4E). A significant feature of the BD70-4017 binding mode is its interaction with the N-linked glycan at position N63 of domain I (Figure 4F). The light-chain residue T70 forms a hydrogen bond with the mannose moiety of this glycan, a

(D) The gene analysis of the antibodies in eight groups. A Sankey diagram was generated to visualize the correspondence between heavy and light chains for the antibody genes in each group, with asterisks indicating the inclusion of control antibodies.
(E and F) Statistical analysis of the number (E) and IC_{50} values (mean ± SEM) (F) for neutralization against the HB29 strain across DMS-classified antibody groups was performed.
See also Figures S2 and S3 and Tables S6 and S7.

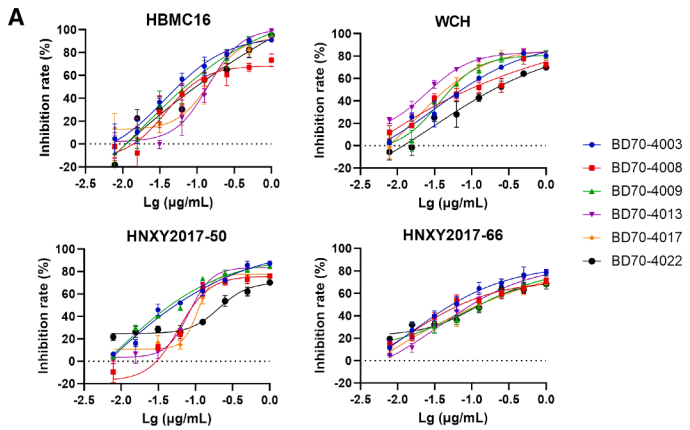

B

Antibody (μg/mL)	authentic virus ($FRNT_{50}$)			
	HBMC16	WCH	HNXY 2017-50	HNXY 2017-66
BD70-4003 (Ⅰ A)	0.062	0.087	0.065	0.070
BD70-4008 (Ⅲ A)	0.149	0.111	0.137	0.109
BD70-4009 (Ⅲ A)	0.078	0.070	0.058	0.138
BD70-4013 (Ⅰ A)	0.137	0.031	0.108	0.126
BD70-4017 (Ⅲ A)	0.126	0.059	0.140	0.155
BD70-4022 (Ⅲ A)	0.111	0.234	0.231	0.143

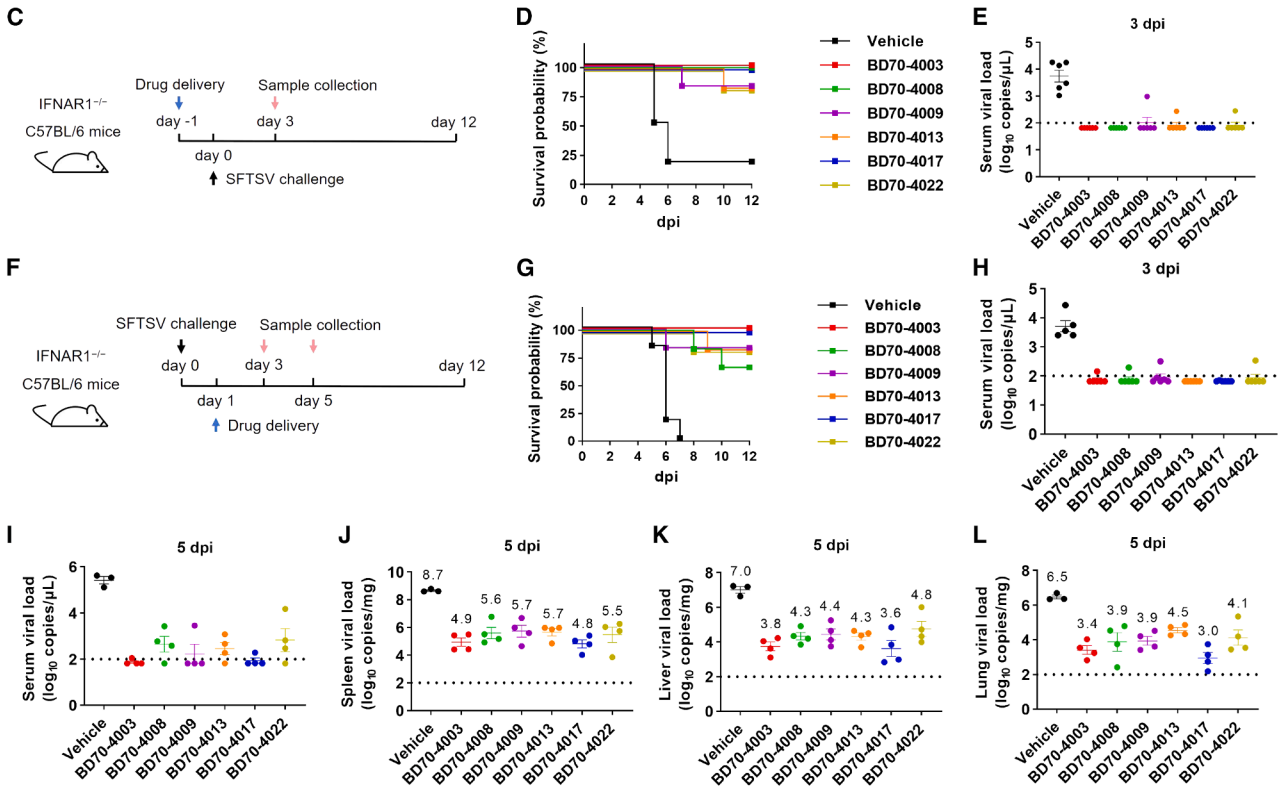

Figure 3. mAb-mediated protection of authentic virus challenge *in vitro* and *in vivo*

(A and B) The neutralization activity of six selected mAbs against four authentic SFTSV viruses. The $FRNT_{50}$ was calculated using the equation of log [inhibitor] versus response-variable slope (four-parameter) method. Data are shown as the mean SD values from three biologically independent replicates.

(C and F) Schematic of the design for the HBMC16 challenge experiment in mice. In prophylactic groups (C), 5 mg/kg mAb was administered intraperitoneally and challenged by HBMC16 intraperitoneally 1 day later (C). In therapeutic groups (F), antibodies were given intraperitoneally 1 day after virus challenge. Each group consists of 6 mice.

(D and G) Survival curves of mice in each group.

(E, H, and I) Viral load in the serum of mice in each group.

(J–L) Viral load (mean ± SD) of mice challenged by HBMC16 in spleen (J), liver (K), or lung (L). Each point corresponds to samples from a mouse. The limit of detection is about 1.81×10^2 copies/g and is shown as the dashed line.

See also Figure S4.

mechanism that may enhance the stability of the complex on the authentic virion surface. Given that domain III acts as a structural cap over the Gc fusion loop, the binding of BD70-4017 likely hinders the exposure of the fusion machinery, thereby preventing the acidification-induced conformational changes required for viral entry.

The structural analysis of BD70-4008 provided a cautionary insight into the interpretation of DMS data. Although DMS

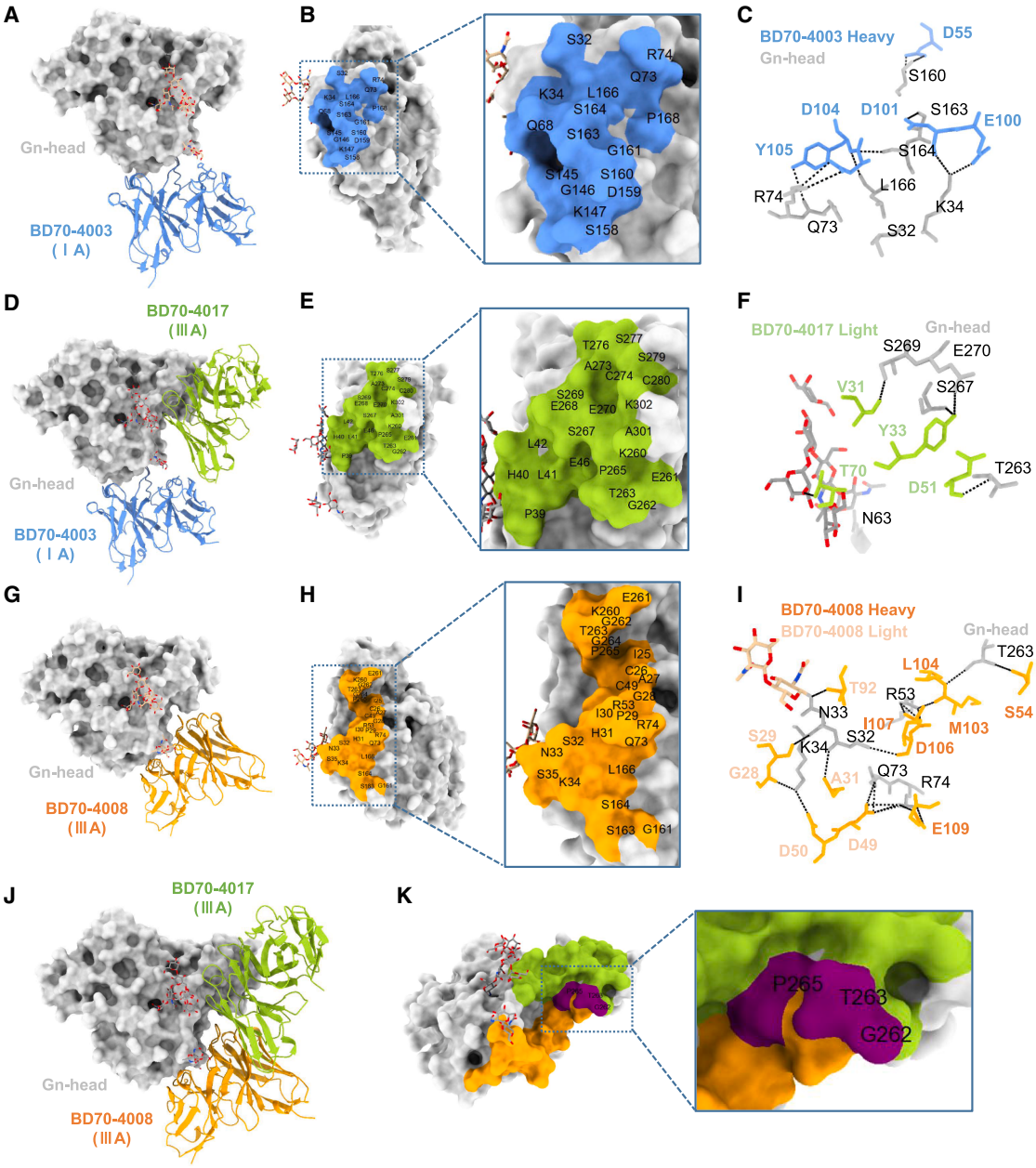

Figure 4. Cryo-EM structure of Gn antibodies bound to HB29-Gn-head

(A, D, G, and J) Aligned structures of BD70-4003 (A), BD70-4003/BD70-4017 (D), BD70-4008 (G), and BD70-4008/BD70-4017 (J) on SFTSV Gn head. BD70-4003, BD70-4008, and BD70-4017 are colored in blue, orange, and green, respectively. Gn head is colored in gray.

(B, E, and H) Surface representation of the contact residues on Gn head interacting with BD70-4003 (B), BD70-4017 (E), and BD70-4008 (H).

(C, F, and I) Interactions between the heavy-chain and light-chain BD70-4003 (C), BD70-4017 (F), and BD70-4008 (I) and Gn head. Residues of Gn head, BD70-4003, BD70-4008, and BD70-4017 are gray, blue, orange, and green, respectively.

(K) The overlapping epitopes of BD70-4008 and BD70-4017 are labeled in purple.

See also Figures S5 and S6 and Table S8.

clustered BD70-4008 into group IIIA along with BD70-4017, the cryo-EM structure revealed that BD70-4008 actually interacts with a hybrid epitope spanning domains I and III (Figures 4G–4I). The discrepancy arose because BD70-4008 possesses relatively few escape residues (Q50, R74, and T263), making its DMS escape profile computationally similar to the domain III-focused BD70-4017. This "grouping bias" highlights that while DMS is a powerful tool for rapid classification, it can underrepresent complex, multi-domain epitopes if only a subset of residues provides strong escape signals. Interestingly, although the amino acid residues on the interacting interface of BD70-4008 and BD70-4017 have a slight overlap, involving

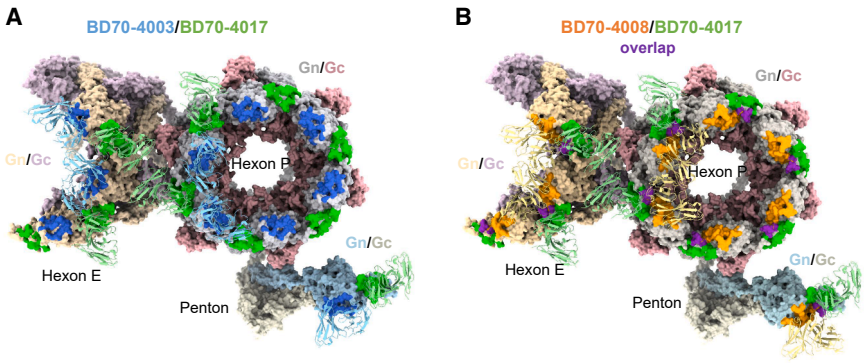

Figure 5. Docking of three antibodies onto the surface of the SFTSV virion

Docking of BD70-4003/BD70-4017 (A) and BD70-4008/BD70-4017 (B) onto the surface of SFTSV virion (PDB: 8I4T). BD70-4003, BD70-4008, and BD70-4017 are colored in blue, orange, and green, respectively. The binding sites of mAbs on the SFTSV virion are labeled with colors within the same palette.

3 residues (G262, T263, and P265), the combination of the two antibodies has little hindering effect on the formation of the Gn head/BD70-4008/BD70-4017 complex (Figures 4J and 4K).

To investigate the neutralization mechanisms of BD70-4003, BD70-4008, and BD70-4017, we superimposed the structures of the BD70-4003/BD70-4017-Gn and BD70-4008/BD70-4017-Gn complexes onto the native SFTSV virion structure. Previous studies have shown that Gn-Gc heterodimers form hexon and penton on the surface of SFTSV virions.[12,42] Our results showed that BD70-4003/BD70-4017 and BD70-4008/BD70-4017 binding sites were located on the surfaces of the hexons or pentons (Figures 5A and 5B). BD70-4003 or BD70-4008 binds to the top side of the authentic SFTSV virion with an orientation nearly perpendicular to the viral membrane, which may be the key factor contributing to the superior affinity and neutralization effects. Although BD70-4017 binds to a more lateral position, its binding is less affected and experiences minimal steric hindrance. This structural complementarity supports the potential for combining these antibodies into a therapeutic cocktail.

DISCUSSION

Currently, the clinical management of SFTS is centered on comprehensive supportive care, including platelet transfusion, intravenous immunoglobulin, and blood purification.[43–45] Due to the lack of specific and effective antiviral drugs, severe cases can rapidly progress to multiple organ failure, particularly in older patients, with significantly increased mortality rates.[46] In this study, we successfully combined pseudovirus screening with authentic virus validation to identify potent mAbs that may serve as SFTSV therapeutics.[32] Compared to authentic viruses, pseudoviruses offer advantages including lower strain restrictions, higher detection throughput, and operational convenience, making them suitable for preliminary efficacy screening. However, we observed that antibody BD70-4017, which displayed relatively modest performance in the pseudovirus system, demonstrated significantly enhanced neutralizing activity against the authentic virus (Figure 1; Table S3), highlighting that the VSV-G-based pseudovirus system cannot completely mimic the surface glycoprotein arrangement of authentic SFTSV. Similar limitations have been previously reported in studies on both SFTSV[15] and hantavirus,[47] and lentiviral-based SFTSV pseudoviruses[48,49] also appear unable to fully recapitulate authentic viral features. Future research should focus on optimizing existing systems or developing novel platforms that accurately mimic the glycoprotein distribution of the authentic virus, thereby enabling high-throughput antibody testing in conventional laboratory settings.

Mapping antibody epitopes is essential for understanding neutralization mechanisms and guiding rational vaccine and therapeutic design. The implementation of a high-resolution DMS platform for bunyavirus antibody characterization represents a significant technical advancement. Traditional epitope mapping methods, such as competitive ELISAs or cross-blocking assays, provide only coarse-grained information about epitope groups. In contrast, DMS provides residue-level specificity, allowing for the immediate identification of potential escape variants and the rational design of antibody cocktails. By comprehensively evaluating the impact of every possible amino acid substitution on antibody binding, researchers can proactively monitor viral antigenic evolution in the field and update therapeutic strategies accordingly. Also, the revision of the SFTSV Gn antigenic landscape into eight specific epitope groups clarifies why previous studies observed varying degrees of protection. For instance, targeting the variable regions of domain III (IIIB) often leads to strain-specific or weak protection compared to the functional interfaces in domain III (IIIA). Specifically, the MAb4-5 (IIIB) is thought to neutralize infection by recognizing a transient intermediate state during membrane fusion. In the prefusion state of mature virions, however, this epitope is masked by adjacent Gn/Gc subunits, most likely causing steric hindrance that restricts binding and limits neutralizing potency.[12] In contrast, BD70-4017 (IIIA) is not subject to such steric constraints (Figure 5). These differences may account for the distinct neutralizing activities observed between the two epitope groups.

The identification of the BD70 series coincides with a burgeoning field of SFTSV immunology characterized by the discovery of several other potent human and murine antibodies.[13–17] Recent studies have introduced several high-performing antibody series, notably the JK series (JK-2 and JK-8),[18] the SD series (SD4, SD12, and SD22),[19] and the ultrapotent ZS1C5.[50] Like BD70-4003, the JK series and SD series primarily target domain I. SD4 and SD22 exhibit picomolar binding affinities (32–83 pM) and have shown 100% protection in mice when given at 20 mg/kg at 3 dpi, representing a potentially wider therapeutic window than the BD70 series if higher doses are used.

The antibody ZS1C5 represents a distinct class of ''interdomain'' neutralizers.[50] Structural analysis has revealed that ZS1C5 bridges domains I and III of the Gn head, mediated by an unusually long CDRH3 of over 17 residues. ZS1C5 exhibits subnanomolar potency and has demonstrated robust protection in both murine and non-human primate (NHP) models, the latter representing a significant milestone for SFTSV therapeutics. While BD70-4003 and BD70-4017 target more traditional domain-specific epitopes, their high efficacy and distinct binding sites make them excellent partners for cocktails, potentially mirroring the success seen with other emerging interdomain-targeting platforms.

In conclusion, the delineation of the SFTSV Gn antigenic landscape and the functional characterization of human mAbs provide a definitive path forward for both therapy and prevention. The integration of high-throughput mutational screening with atomic-level structural analysis has resolved long-standing questions regarding epitope-function relationships, identifying the Gn-head domains I and III as the primary targets for neutralizing intervention. The unique structural insights provided by the DMS-cryo-EM synergy not only advance the development of SFTSV-specific drugs but also establish a generalizable model for responding to other emerging tick-borne viruses. These findings, coupled with the demonstration of 100% *in vivo* protection, provide a robust foundation for the rational design of universal vaccines for SFTSV and its related pathogens.

Limitations of the study

Our study has established a powerful framework for discovering bunyavirus antibodies using DMS and identified promising therapeutic candidates, but some limitations remain. First, the binding sites of some mAbs cannot be efficiently identified by DMS due to a weak escape signal or high noise from non-epitope sites, and DMS-based unsupervised clustering is limited by the size of the mAb collection in this study. These epitope mapping results could be complemented by structural analyses. Second, the conclusions derived from pseudovirus-based neutralization assays cannot always be directly translated to inhibition against a live virus or efficacy *in vivo*, highlighting the necessity of further validation. Lastly, the effectiveness of BD70-4003 or BD70-4017 against advanced-stage infections has not been fully demonstrated, as patients typically present for treatment multiple days after symptoms emerge. Further pre-clinical and clinical research should prioritize refining dosing protocols and assessing long-term safety and efficacy.

RESOURCE AVAILABILITY

Lead contact

Requests for further information, resources, and reagents should be directed to and will be fulfilled by the lead contact, Yunlong Cao (yunlongcao@pku.edu.cn).

Materials availability

All unique reagents generated in this study are available from the lead contact with a completed materials transfer agreement.

Data and code availability

Sequences of the mAbs involved in this study are available in Table S6, and processed mutation escape data have been deposited at Zenodo and are publicly available as of the date of publication at https://doi.org/10.5281/zenodo.19045315. Cryo-EM density maps have been deposited in the Electron Microscopy Data Bank with accession codes EMDB: EMD-67524, EMD-67541, EMD-67539, and EMD-67523. Structural coordinates have been deposited in the Protein Data Bank with accession codes PDB: 21AQ, 21AV, 21AU, and 21AO. Any additional information required to reanalyze the data reported in this paper is available from the lead contact upon request.

ACKNOWLEDGMENTS

We thank Yantai Qishan Hospital for the assistance in recruiting SFTSV-infected convalescents and collecting samples. We thank Yuhang Wang from Changping Laboratory for support with structural analysis. We thank Nanjing GenScript Biotechnology for the technical assistance on the purification of mAbs. This project is financially supported by Changping Laboratory (2025D-04-01).

AUTHOR CONTRIBUTIONS

Y.C. designed the study. Y.C., Q.W., and J.L. wrote the manuscript with input from all authors. Y.C. and F.S. coordinated the expression and characterization of the neutralizing antibodies. F.J., Q.W., and H.S. performed and analyzed the yeast display screening experiments. Q.W., Y.Y., J.W., L.Y., and Y.W. performed the neutralizing antibody expression and characterization, including pseudovirus neutralization assays and ELISAs. Q.W., M.M., and F.J. performed and analyzed the antigen-specific single B cell V(D)J sequencing. Y.W. and Q.W. performed the structural analyses. W.L., H.L., and A.H. performed and coordinated the authentic virus neutralization and animal experiments. Y.L. and L.Z. recruited the SFTSV convalescents.

DECLARATION OF INTERESTS

Provisional patents related to the antibodies identified in this paper have been filed. Y.C. is the co-founder of Singlomics Biopharmaceuticals.

STAR★METHODS

Detailed methods are provided in the online version of this paper and include the following:

- KEY RESOURCES TABLE
- EXPERIMENTAL MODEL AND STUDY PARTICIPANT DETAILS
  - Cells
  - SFTSV VSV-based pseudovirus
  - Authentic SFTSV virus
  - IFNAR−/− mice
- METHOD DETAILS
  - Plasma donors
  - Antigen-specific cell sorting, V(D)J sequencing, and data analysis
  - Monoclonal antibody expression and purification
  - ELISA
  - Surface plasmon resonance
  - Pseudovirus neutralization assay
  - DMS library construction
  - High-throughput antibody-escape profiling
  - Processing of DMS data
  - Authentic virus neutralization assay
  - *In vivo* SFTSV challenge experiment
  - RT-qPCR assay
  - Protein expression and purification for structural analysis
  - Cryo-EM sample preparation, data collection and model building
- QUANTIFICATION AND STATISTICAL ANALYSIS

SUPPLEMENTAL INFORMATION

Supplemental information can be found online at https://doi.org/10.1016/j.celrep.2026.117248.

Received: December 5, 2025
Revised: February 9, 2026
Accepted: March 19, 2026

REFERENCES

1. Yu, X.J., Liang, M.F., Zhang, S.Y., Liu, Y., Li, J.D., Sun, Y.L., Zhang, L., Zhang, Q.F., Popov, V.L., Li, C., et al. (2011). Fever with thrombocytopenia associated with a novel bunyavirus in China. N. Engl. J. Med. *364*, 1523–1532. https://doi.org/10.1056/NEJMoa1010095.

2. Liu, W., Lu, Q.B., Cui, N., Li, H., Wang, L.Y., Liu, K., Yang, Z.D., Wang, B.J., Wang, H.Y., Zhang, Y.Y., et al. (2013). Case-fatality ratio and effectiveness of ribavirin therapy among hospitalized patients in china who had severe fever with thrombocytopenia syndrome. Clin. Infect. Dis. *57*, 1292–1299. https://doi.org/10.1093/cid/cit530.

3. Liu, Q., He, B., Huang, S.Y., Wei, F., and Zhu, X.Q. (2014). Severe fever with thrombocytopenia syndrome, an emerging tick-borne zoonosis. Lancet Infect. Dis. *14*, 763–772. https://doi.org/10.1016/S1473-3099(14)70718-2.

4. Yang, T., Huang, H., Jiang, L., and Li, J. (2022). Overview of the immunological mechanism underlying severe fever with thrombocytopenia syndrome (Review). Int. J. Mol. Med. *50*, 118. https://doi.org/10.3892/ijmm.2022.5174.

5. Wang, Y., Song, Z., Wei, X., Yuan, H., Xu, X., Liang, H., and Wen, H. (2022). Clinical laboratory parameters and fatality of Severe fever with thrombocytopenia syndrome patients: A systematic review and meta-analysis. PLoS Negl. Trop. Dis. *16*, e0010489. https://doi.org/10.1371/journal.pntd.0010489.

6. Li, H., Lu, Q.-B., Xing, B., Zhang, S.-F., Liu, K., Du, J., Li, X.-K., Cui, N., Yang, Z.-D., Wang, L.-Y., et al. (2018). Epidemiological and clinical features of laboratory-diagnosed severe fever with thrombocytopenia syndrome in China, 2011–17: a prospective observational study. Lancet Infect. Dis. *18*, 1127–1137. https://doi.org/10.1016/s1473-3099(18)30293-7.

7. Egizi, A., Bulaga-Seraphin, L., Alt, E., Bajwa, W.I., Bernick, J., Bickerton, M., Campbell, S.R., Connally, N., Doi, K., Falco, R.C., et al. (2020). First glimpse into the origin and spread of the Asian longhorned tick, Haemaphysalis longicornis, in the United States. Zoonoses Public Health *67*, 637–650. https://doi.org/10.1111/zph.12743.

8. Miao, D., Dai, K., Zhao, G.P., Li, X.L., Shi, W.Q., Zhang, J.S., Yang, Y., Liu, W., and Fang, L.Q. (2020). Mapping the global potential transmission hotspots for severe fever with thrombocytopenia syndrome by machine learning methods. Emerg. Microbes Infect. *9*, 817–826. https://doi.org/10.1080/22221751.2020.1748521.

9. Zhang, X., Zhao, C., Cheng, C., Zhang, G., Yu, T., Lawrence, K., Li, H., Sun, J., Yang, Z., Ye, L., et al. (2022). Rapid Spread of Severe Fever with Thrombocytopenia Syndrome Virus by Parthenogenetic Asian Longhorned Ticks. Emerg. Infect. Dis. *28*, 363–372. https://doi.org/10.3201/eid2802.211532.

10. Spiegel, M., Plegge, T., and Pöhlmann, S. (2016). The Role of Phlebovirus Glycoproteins in Viral Entry, Assembly and Release. Viruses *8*, 202, *8*. https://doi.org/10.3390/v8070202.

11. Halldorsson, S., Behrens, A.J., Harlos, K., Huiskonen, J.T., Elliott, R.M., Crispin, M., Brennan, B., and Bowden, T.A. (2016). Structure of a phleboviral envelope glycoprotein reveals a consolidated model of membrane fusion. Proc. Natl. Acad. Sci. USA *113*, 7154–7159. https://doi.org/10.1073/pnas.1603827113.

12. Du, S., Peng, R., Xu, W., Qu, X., Wang, Y., Wang, J., Li, L., Tian, M., Guan, Y., Wang, J., et al. (2023). Cryo-EM structure of severe fever with thrombocytopenia syndrome virus. Nat. Commun. *14*, 6333. https://doi.org/10.1038/s41467-023-41804-7.

13. Wu, Y., Zhu, Y., Gao, F., Jiao, Y., Oladejo, B.O., Chai, Y., Bi, Y., Lu, S., Dong, M., Zhang, C., et al. (2017). Structures of phlebovirus glycoprotein Gn and identification of a neutralizing antibody epitope. Proc. Natl. Acad. Sci. USA *114*, E7564–E7573. https://doi.org/10.1073/pnas.1705176114.

14. Kim, K.H., Kim, J., Ko, M., Chun, J.Y., Kim, H., Kim, S., Min, J.Y., Park, W.B., Oh, M.D., and Chung, J. (2019). An anti-Gn glycoprotein antibody from a convalescent patient potently inhibits the infection of severe fever with thrombocytopenia syndrome virus. PLoS Pathog. *15*, e1007375. https://doi.org/10.1371/journal.ppat.1007375.

15. Ren, X., Sun, J., Kuang, W., Yu, F., Wang, B., Wang, Y., Deng, W., Xu, Z., Yang, S., Wang, H., et al. (2024). A broadly protective antibody targeting glycoprotein Gn inhibits severe fever with thrombocytopenia syndrome virus infection. Nat. Commun. *15*, 7009. https://doi.org/10.1038/s41467-024-51108-z.

16. Yang, P., Wu, X., Shang, H., Sun, Z., Wang, Z., Song, Z., Yuan, H., Deng, F., Shen, S., Guo, Y., and Zhang, N. (2024). Molecular mechanism and structure-guided humanization of a broadly neutralizing antibody against SFTSV. PLoS Pathog. *20*, e1012550. https://doi.org/10.1371/journal.ppat.1012550.

17. Wu, X., Moming, A., Zhang, Y., Wang, Z., Zhang, T., Fu, L., Qian, J., Ni, J., Hu, S., Tang, S., et al. (2024). Identification and characterization of three monoclonal antibodies targeting the SFTSV glycoprotein and displaying a broad spectrum recognition of SFTSV-related viruses. PLoS Negl. Trop. Dis. *18*, e0012216. https://doi.org/10.1371/journal.pntd.0012216.

18. Zhang, S., Shang, H., Han, S., Li, J., Peng, X., Wu, Y., Yang, X., Leng, Y., Wang, F., Cui, N., et al. (2025). Discovery and characterization of potent broadly neutralizing antibodies from human survivors of severe fever with thrombocytopenia syndrome. EBioMedicine *111*, 105481. https://doi.org/10.1016/j.ebiom.2024.105481.

19. Quan, C., Nie, K., Ma, D., Su, C., Li, L., Zheng, W., Yin, C., Wang, Y., Yang, P., Peng, D., et al. (2025). Molecular mechanism of potently neutralizing human monoclonal antibodies against severe fever with thrombocytopenia virus infection. J. Virol. *99*, e0053325. https://doi.org/10.1128/jvi.00533-25.

20. Greaney, A.J., Starr, T.N., Gilchuk, P., Zost, S.J., Binshtein, E., Loes, A.N., Hilton, S.K., Huddleston, J., Eguia, R., Crawford, K.H.D., et al. (2021). Complete Mapping of Mutations to the SARS-CoV-2 Spike Receptor-Binding Domain that Escape Antibody Recognition. Cell Host Microbe *29*, 44–57.e9. https://doi.org/10.1016/j.chom.2020.11.007.

21. Cao, Y., Wang, J., Jian, F., Xiao, T., Song, W., Yisimayi, A., Huang, W., Li, Q., Wang, P., An, R., et al. (2022). Omicron escapes the majority of existing SARS-CoV-2 neutralizing antibodies. Nature *602*, 657–663. https://doi.org/10.1038/s41586-021-04385-3.

22. Jian, F., Wang, J., Yisimayi, A., Song, W., Xu, Y., Chen, X., Niu, X., Yang, S., Yu, Y., Wang, P., et al. (2025). Evolving antibody response to SARS-CoV-2 antigenic shift from XBB to JN.1. Nature *637*, 921–929. https://doi.org/10.1038/s41586-024-08315-x.

23. Yisimayi, A., Song, W., Wang, J., Jian, F., Yu, Y., Chen, X., Xu, Y., Yang, S., Niu, X., Xiao, T., et al. (2024). Repeated Omicron exposures override ancestral SARS-CoV-2 immune imprinting. Nature *625*, 148–156. https://doi.org/10.1038/s41586-023-06753-7.

24. Cao, Y., Jian, F., Wang, J., Yu, Y., Song, W., Yisimayi, A., Wang, J., An, R., Chen, X., Zhang, N., et al. (2023). Imprinted SARS-CoV-2 humoral immunity induces convergent Omicron RBD evolution. Nature *614*, 521–529. https://doi.org/10.1038/s41586-022-05644-7.

25. Cao, Y., Yisimayi, A., Jian, F., Song, W., Xiao, T., Wang, L., Du, S., Wang, J., Li, Q., Chen, X., et al. (2022). BA.2.12.1, BA.4 and BA.5 escape

antibodies elicited by Omicron infection. Nature *608*, 593–602. https://doi.org/10.1038/s41586-022-04980-y.

26. Cao, Y., Jian, F., Zhang, Z., Yisimayi, A., Hao, X., Bao, L., Yuan, F., Yu, Y., Du, S., Wang, J., et al. (2022). Rational identification of potent and broad sarbecovirus-neutralizing antibody cocktails from SARS convalescents. Cell Rep. *41*, 111845. https://doi.org/10.1016/j.celrep.2022.111845.
27. Jian, F., Wec, A.Z., Feng, L., Yu, Y., Wang, L., Wang, P., Yu, L., Wang, J., Hou, J., Berrueta, D.M., et al. (2025). Viral evolution prediction identifies broadly neutralizing antibodies to existing and prospective SARS-CoV-2 variants. Nat. Microbiol. *10*, 2003–2017. https://doi.org/10.1038/s41564-025-02030-7.
28. Chung, H., Kim, E., Kwon, B., Cho, Y.G., Bae, S., Jung, J., Kim, M.J., Chong, Y.P., Kim, S.H., Lee, S.O., et al. (2022). Kinetics of Glycoprotein-Specific Antibody Response in Patients with Severe Fever with Thrombocytopenia Syndrome. Viruses *14*, 256. https://doi.org/10.3390/v14020256.
29. Li, J.C., Ding, H., Wang, G., Zhang, S., Yang, X., Wu, Y.X., Peng, X.F., Zhang, X.A., Yang, Z.D., Cui, N., et al. (2023). Dynamics of neutralizing antibodies against severe fever with thrombocytopenia syndrome virus. Int. J. Infect. Dis. *134*, 95–98. https://doi.org/10.1016/j.ijid.2023.05.018.
30. Fu, Y., Li, S., Zhang, Z., Man, S., Li, X., Zhang, W., Zhang, C., and Cheng, X. (2016). Phylogeographic analysis of severe fever with thrombocytopenia syndrome virus from Zhoushan Islands, China: implication for transmission across the ocean. Sci. Rep. *6*, 19563. https://doi.org/10.1038/srep19563.
31. Yun, S.M., Park, S.J., Park, S.W., Choi, W., Jeong, H.W., Choi, Y.K., and Lee, W.J. (2017). Molecular genomic characterization of tick- and human-derived severe fever with thrombocytopenia syndrome virus isolates from South Korea. PLoS Negl. Trop. Dis. *11*, e0005893. https://doi.org/10.1371/journal.pntd.0005893.
32. Xu, J., Liu, Y., Zhang, F., Wang, X., Huang, W., Wu, Y., Li, B., Zhuang, J., Bing, Y., Wang, Y., and Qiao, Y. (2022). Analysis of cross neutralizing activity of antibodies from sera of severe fever with thrombocytopenia syndrome patients to deal with different genotype strains. Front. Microbiol. *13*, 1020545. https://doi.org/10.3389/fmicb.2022.1020545.
33. Guo, X., Zhang, L., Zhang, W., Chi, Y., Zeng, X., Li, X., Qi, X., Jin, Q., Zhang, X., Huang, M., et al. (2013). Human antibody neutralizes severe Fever with thrombocytopenia syndrome virus, an emerging hemorrhagic Fever virus. Clin. Vaccine Immunol. *20*, 1426–1432. https://doi.org/10.1128/CVI.00222-13.
34. Park, S.Y., Choi, W., Chong, Y.P., Park, S.W., Wang, E.B., Lee, W.J., Jee, Y., Kwon, S.W., and Kim, S.H. (2016). Use of Plasma Therapy for Severe Fever with Thrombocytopenia Syndrome Encephalopathy. Emerg. Infect. Dis. *22*, 1306–1308. https://doi.org/10.3201/eid2207.151791.
35. Choi, S., Kim, M.C., Kwon, J.S., Kim, J.Y., Lee, K.H., and Kim, S.H. (2018). Case Report: Use of Plasma Exchange Followed by Convalescent Plasma Therapy in a Critically Ill Patient with Severe Fever and Thrombocytopenia Syndrome-Associated Encephalopathy: Cytokine/Chemokine Concentrations, Viral Loads, and Antibody Responses. Am. J. Trop. Med. Hyg. *99*, 1466–1468. https://doi.org/10.4269/ajtmh.17-0766.
36. Starr, T.N., Greaney, A.J., Addetia, A., Hannon, W.W., Choudhary, M.C., Dingens, A.S., Li, J.Z., and Bloom, J.D. (2021). Prospective mapping of viral mutations that escape antibodies used to treat COVID-19. Science *371*, 850–854. https://doi.org/10.1126/science.abf9302.
37. Starr, T.N., Greaney, A.J., Dingens, A.S., and Bloom, J.D. (2021). Complete map of SARS-CoV-2 RBD mutations that escape the monoclonal antibody LY-CoV555 and its cocktail with LY-CoV016. Cell Rep. Med. *2*, 100255. https://doi.org/10.1016/j.xcrm.2021.100255.
38. Sivelle, C., Sierocki, R., Lesparre, Y., Lomet, A., Quintilio, W., Dubois, S., Correia, E., Moro, A.M., Maillère, B., and Nozach, H. (2023). Combining deep mutational scanning to heatmap of HLA class II binding of immunogenic sequences to preserve functionality and mitigate predicted immunogenicity. Front. Immunol. *14*, 1197919. https://doi.org/10.3389/fimmu.2023.1197919.
39. Chang, Z., Gao, D., Liao, L., Sun, J., Zhang, G., Zhang, X., Wang, F., Li, C., Oladejo, B.O., Li, S., et al. (2024). Bispecific antibodies targeting two glycoproteins on SFTSV exhibit synergistic neutralization and protection in a mouse model. Proc. Natl. Acad. Sci. USA *121*, e2400163121. https://doi.org/10.1073/pnas.2400163121.
40. Zhang, L., Peng, X., Wang, Q., Li, J., Lv, S., Han, S., Zhang, L., Ding, H., Wang, C.Y., Xiao, G., et al. (2023). CCR2 is a host entry receptor for severe fever with thrombocytopenia syndrome virus. Sci. Adv. *9*, eadg6856. https://doi.org/10.1126/sciadv.adg6856.
41. Wang, L., Wang, J., Zhang, J., Wang, X., Cao, W., Yang, L., Wu, Y., Li, B., and Qiao, Y. (2025). Weakened invasion of severe fever with thrombocytopenia syndrome bunyavirus beneficial to its immune escape by multi-site mutation of glycoprotein. Mol. Genet. Genomics. *300*, 109. https://doi.org/10.1007/s00438-025-02319-6.
42. Sun, Z., Cheng, J., Bai, Y., Cao, L., Xie, D., Deng, F., Zhang, X., Rao, Z., and Lou, Z. (2023). Architecture of severe fever with thrombocytopenia syndrome virus. Protein Cell *14*, 914–918. https://doi.org/10.1093/procel/pwad019.
43. Zhai, Y., Li, H., Xia, P., Jiang, Y., Tong, H., Zhou, D., Jiang, C., Liu, Y., and Wang, J. (2024). Intravenous immunoglobulin-based adjuvant therapy for severe fever with thrombocytopenia syndrome: A single-center retrospective cohort study. J. Med. Virol. *96*, e70017. https://doi.org/10.1002/jmv.70017.
44. Song, X., Xu, X., Ren, X., Ruan, X., and Bo, J. (2024). Therapeutic plasma exchange combined with ribavirin to rescue critical SFTS patients. J. Clin. Apher. *39*, e22131. https://doi.org/10.1002/jca.22131.
45. Wang, W., Zhang, A., Wu, Q., Zhu, L., and Yang, J. (2022). Epidemiological and Clinical Characteristics of Severe Fever with Thrombocytopenia Syndrome in Southern Anhui Province, China, 2011-2020. Jpn. J. Infect. Dis. *75*, 133–139. https://doi.org/10.7883/yoken.JJID.2021.391.
46. Zu, Z., Hu, Y., Zheng, X., Chen, C., Zhao, Y., Jin, Y., Lin, H., and He, N. (2022). A ten-year assessment of the epidemiological features and fatal risk factors of hospitalised severe fever with thrombocytopenia syndrome in Eastern China. Epidemiol. Infect. *150*, e131. https://doi.org/10.1017/S0950268822001108.
47. Engdahl, T.B., Binshtein, E., Brocato, R.L., Kuzmina, N.A., Principe, L.M., Kwilas, S.A., Kim, R.K., Chapman, N.S., Porter, M.S., Guardado-Calvo, P., et al. (2023). Antigenic mapping and functional characterization of human New World hantavirus neutralizing antibodies. eLife *12*, e81743. https://doi.org/10.7554/eLife.81743.
48. Hofmann, H., Li, X., Zhang, X., Liu, W., Kühl, A., Kaup, F., Soldan, S.S., González-Scarano, F., Weber, F., He, Y., and Pöhlmann, S. (2013). Severe fever with thrombocytopenia virus glycoproteins are targeted by neutralizing antibodies and can use DC-SIGN as a receptor for pH-dependent entry into human and animal cell lines. J. Virol. *87*, 4384–4394. https://doi.org/10.1128/JVI.02628-12.
49. Chen, R., Huang, W., and Wang, Y. (2023). Pseudotyped Virus for Bandavirus. Adv. Exp. Med. Biol. *1407*, 265–277. https://doi.org/10.1007/978-981-99-0113-5_14.
50. Bi, J., Dai, Z., Hong, X., Zhang, Y., Lu, S., Wang, Q., Liu, Y., Li, X., Li, M., Song, G., et al. (2026). A potent interdomain epitope-targeting antibody protects against SFTSV in mice and non-human primates. Vita. https://doi.org/10.15302/vita.2025.12.0002.
51. Liebschner, D., Afonine, P.V., Baker, M.L., Bunkóczi, G., Chen, V.B., Croll, T.I., Hintze, B., Hung, L.W., Jain, S., McCoy, A.J., et al. (2019). Macromolecular structure determination using X-rays, neutrons and electrons: recent developments in Phenix. Acta Crystallogr. D Struct. Biol. *75*, 861–877. https://doi.org/10.1107/S2059798319011471.
52. Emsley, P., Lohkamp, B., Scott, W.G., and Cowtan, K. (2010). Features and development of Coot. Acta Crystallogr. D Biol. Crystallogr. *66*, 486–501. https://doi.org/10.1107/S0907444910007493.

53. Gietz, R.D., and Schiestl, R.H. (2007). High-efficiency yeast transformation using the LiAc/SS carrier DNA/PEG method. Nat. Protoc. *2*, 31–34. https://doi.org/10.1038/nprot.2007.13.

54. Du, S., Cao, Y., Zhu, Q., Yu, P., Qi, F., Wang, G., Du, X., Bao, L., Deng, W., Zhu, H., et al. (2020). Structurally Resolved SARS-CoV-2 Antibody Shows High Efficacy in Severely Infected Hamsters and Provides a Potent Cocktail Pairing Strategy. Cell *183*, 1013–1023.e13. https://doi.org/10.1016/j.cell.2020.09.035.

55. Du, S., Liu, P., Zhang, Z., Xiao, T., Yasimayi, A., Huang, W., Wang, Y., Cao, Y., Xie, X.S., and Xiao, J. (2021). Structures of SARS-CoV-2 B.1.351 neutralizing antibodies provide insights into cocktail design against concerning variants. Cell Res. *31*, 1130–1133. https://doi.org/10.1038/s41422-021-00555-0.

56. Punjani, A., Rubinstein, J.L., Fleet, D.J., and Brubaker, M.A. (2017). cryoSPARC: algorithms for rapid unsupervised cryo-EM structure determination. Nat. Methods *14*, 290–296. https://doi.org/10.1038/nmeth.4169.

57. Pettersen, E.F., Goddard, T.D., Huang, C.C., Couch, G.S., Greenblatt, D.M., Meng, E.C., and Ferrin, T.E. (2004). UCSF Chimera–a visualization system for exploratory research and analysis. J. Comput. Chem. *25*, 1605–1612. https://doi.org/10.1002/jcc.20084.

58. Pettersen, E.F., Goddard, T.D., Huang, C.C., Meng, E.C., Couch, G.S., Croll, T.I., Morris, J.H., and Ferrin, T.E. (2021). UCSF ChimeraX: Structure visualization for researchers, educators, and developers. Protein Sci. *30*, 70–82. https://doi.org/10.1002/pro.3943.

STAR★METHODS

KEY RESOURCES TABLE

REAGENT or RESOURCE	SOURCE	IDENTIFIER
Antibodies		
FITC anti-human CD19 antibody	BioLegend	Cat#302206; RRID:AB_314236
Brilliant Violet 421™ anti-human CD27 antibody	BioLegend	Cat# 302824; RRID:AB_11150782
PE/Cyanine7 anti-human IgM antibody	BioLegend	Cat#314532; RRID:AB_2566485
HRP-conjugated goat anti-human IgG	Jackson ImmunoResearch Labs	Cat#109-035-003; RRID:AB_2337577
APC anti-HA.11 Epitope Tag antibody	BioLegend	Cat#901524; RRID:AB_2734658
FITC-conjugated chicken anti-cMyc antibody	Immunology Consultants Laboratory, Inc.	Cat#CMYC-45F
PE-conjugated goat anti-human IgG	Jackson ImmunoResearch Labs	Cat#109-115-098; RRID:AB_2337675
HRP-conjugated anti-mouse secondary antibody	Applygen	Cat#C1308
Bacterial and virus strains		
E. coli DH5α	Tsingke	TSC-C01-96
DH10Bac *E. coli*	Invitrogen	Cat#10359-016
HBMC16	This study	AQX34652.1
WCH/97/HN/China/2011	This study	AFH88227.1
HNXY2017-50	This study	XQW45243.1
HNXY2017-66	This study	XQW45244.1
Chemicals, peptides, and recombinant proteins		
Polyethylenimine	Yeasen	Cat#40816ES03
OPM-293 ProFeed	OPM Biosciences	F081918-001
LabPAGE 4–20% 15 Wells	LabLead	Cat#P42015
Tetramethylbenzidine (TMB) substrate	Solarbio	Cat#PR1200
D-luciferin substrate	PerkinElmer	Cat#6066769
DAB substrate	TIANGEN	Cat#PA110
HB29-Gn protein (His-AVI Tag)	This study	N/A
HB29-Gc protein (His-AVI Tag)	This study	N/A
Critical commercial assays		
MoFlo Astrios EQ Cell Sorter	Beckman Coulter	N/A
EasySep™ Human CD19 Positive Selection Kit II	BioLegend	Cat#392508
Chromium Single Cell V(D)J Enrichment Kit,Human B Cell	10x Genomics	PN-1000016
Chromium Next GEM Chip G Single Cell Kit	10x Genomics	PN-1000120
Protein A magnetic beads	GenScript	L00695
NanoDrop	Thermo Fisher	840–317400
Biacore 8K	Cytiva	N/A
Series S Sensor Chip Protein A	Cytiva	Cat#29127556
Microplate reader	PerkinElmer	HH3400
AMPure XP beads	Beckman Coulter	Cat#A63882
BD FACSAria™ III	BD Biosciences	N/A
RNAprep Pure Cell Kit	TIANGEN	Cat#DP430
Superdex 200 Increase 10/300 GL	Cytiva	Cat#28990944
PE-streptavidin	BioLegend	Cat#405204
APC-streptavidin	BioLegend	Cat#405207
Deposited data		
Mutation escape data	Zenodo	https://doi.org/10.5281/zenodo.19045315

(*Continued on next page*)

Continued		
REAGENT or RESOURCE	SOURCE	IDENTIFIER
Local refinement of BD70-4003 Fab in complex of SFTSV Gn head	This study	PDB ID 21AO, EMD-67523
Local refinement of BD70-4008 Fab in complex of SFTSV Gn head	This study	PDB ID 21AQ, EMD-67524
Local refinement of BD70-4003/BD70-4017 Fab in complex of SFTSV Gn head	This study	PDB ID 21AU, EMD-67539
Local refinement of BD70-4008/BD70-4017 Fab in complex of SFTSV Gn head	This study	PDB ID 21AV, EMD-67541
Experimental models: Cell lines		
HEK293F	ThermoFisher	Cat#R79007
Huh-7	JCRB	Cat#0403
Vero	ATCC	CCL-81
Experimental models: Organisms/strains		
Saccharomyces cerevisiae strain EBY100	ATCC	MYA-4941
Oligonucleotides		
TotalSeq™-C0971 Streptavidin	BioLegend	Cat#405271
TotalSeq™-C0972 Streptavidin	BioLegend	Cat#405273
TotalSeq™-C0973 Streptavidin	BioLegend	Cat#405275
TotalSeq™-C0974 Streptavidin	BioLegend	Cat#405277
TotalSeq™-C0975 Streptavidin	BioLegend	Cat#405279
Recombinant DNA		
pVSV-SFTSV-G	Xu et al. [32]	N/A
BD70-4003 Fab, pcDNA	This study	N/A
BD70-4008 Fab, pcDNA	This study	N/A
BD70-4017 Fab, pcDNA	This study	N/A
Software and algorithms		
FlowJo™ (version 10.8)	BD Biosciences	https://www.flowjo.com
Biacore Insight Evaluation Software	Cytiva	https://www.cytivalifesciences.com
Summit 6.0	Beckman Coulter	https://www.beckmancoulter.com
Cell Ranger (v6.1.1)	10x Genomics	https://www.10xgenomics.com
Prism (v9.0.1)	GraphPad	https://www.graphpad.com
cryoSPARC (v4.7.1)	Structura Bio	https://structura.bio
ChimeraX (v1.7)	UCSF	https://www.cgl.ucsf.edu
Smart EPU software	Thermo Fisher	https://www.thermofisher.cn
PHENIX	Liebschner et al. [51]	https://www.phenix-online.org
COOT	Emsley et al. [52]	https://www2.mrc-lmb.cam.ac.uk/Personal/pemsley/coot

EXPERIMENTAL MODEL AND STUDY PARTICIPANT DETAILS

Cells

For neutralization assays, Huh-7 cells (JCRB, Cat#0403) and Vero cells (ATCC, CCL-81) were cultured in DMEM supplemented with 10% FBS, maintained at 37°C in an incubator supplied with 8% CO2. The above cell lines were commercially sourced and tested negative for mycoplasma contamination by qPCR.

SFTSV VSV-based pseudovirus

The SFTSV pseudovirus was constructed as previously described using VSV pseudotyped virus (G*ΔG-VSV).[32] Pseudovirus carrying glycoprotein of SFTSV HB29, HN20, HN13, SPL030A, SD4, G/K/2012, WCH, HBMC16, and AHL were constructed and used, as described previously.[32]

Authentic SFTSV virus

SFTSV HBMC16, WCH/97/HN/China/2011, HNXY2017-50, and HNXY2017-66 were stored in the State Key Laboratory of Pathogen and Biosecurity of Academy of Military Medical Sciences. The virus load of the cells was determined using a standard 50% focus reduction neutralization test $FRNT_{50}$ assay.

IFNAR−/− mice

Specific-pathogen-free, 6 to 8-week-old IFNAR−/− C57BL6/J mice (18-20g) were raised by the State Key Laboratory of Pathogen and Biosecurity of Academy of Military Medical Sciences as previously described.[18] All animal experiments were performed using female mice to minimize hormonal variations associated with the estrous cycle, in accordance with established animal welfare guidelines. Animal experiment was performed in accordance with the National Institutes of Health guidelines under protocols approved by the Institutional Animal Care and Use Committee (IACUC-IME-2021-003).

METHOD DETAILS

Plasma donors

Blood samples were collected from 12 convalescent individuals previously infected with SFTSV. All plasma-related experiments were approved by the Ethics Committee of Beijing Ditan Hospital, Capital Medical University (approval no. DTEC-KY2022-022-01). Written informed consent was obtained from all participants in accordance with the Declaration of Helsinki, permitting the collection, storage, and research use of clinical samples, as well as publication of resulting data.

Whole blood samples were diluted 1:1 with PBS containing 2% FBS and subjected to Ficoll (Cytiva, 17-1440-03) density gradient centrifugation to separate plasma and PBMCs. Plasma was collected from the upper layer, while cells at the interface were harvested for PBMC isolation. PBMCs were further processed by centrifugation, red blood cell lysis (Invitrogen eBioscience 1× RBC Lysis Buffer, 00-4333-57), and washing steps. Samples not used immediately were were stored in FBS (Gibco) containing 10% DMSO (Sigma) in liquid nitrogen. Cryopreserved PBMCs were thawed in DPBS containing 2% FBS (Stemcell, 07905) prior to use.

Antigen-specific cell sorting, V(D)J sequencing, and data analysis

PBMCs were processed using the EasySep Human CD19 Positive Selection Kit II (STEMCELL, 17854) to isolate $CD19^+$ B cells. Cells were stained with FITC anti-human CD19 (BioLegend, 302206, clone HIB19), Brilliant Violet 421 anti-human CD27 (BioLegend, 302824, clone O323), and PE/Cyanine7 anti-human IgM (BioLegend, 314532, clone MHM-88). For antigen labeling, biotinylated SFTSV HB29-Gn or HB29-Gc protein was conjugated with PE-streptavidin (BioLegend, 405204) and APC-streptavidin (BioLegend, 405207), respectively. Biotinylated ovalbumin (OVA) conjugated with streptavidin served as a negative control. Specifically, HB29-Gn and HB29-Gc were labeled with distinct barcodes: Gn was conjugated with TotalSeq-C0971 and TotalSeq-C0972 Streptavidin (BioLegend, 405271 and 405273), while Gc was conjugated with TotalSeq-C0973 and TotalSeq-C0974 Streptavidin (BioLegend, 405275 and 405277) to enable sequencing-adapted sorting. OVA was labeled with TotalSeq-C0975 Streptavidin (BioLegend, 405279). Cells were incubated on ice in the dark for 30 min and washed twice. Dead cells were excluded by 7-AAD staining (Invitrogen, 00-6993-50). $7\text{-}AAD^-$, $CD19^+$, $CD27^+$, IgM^-, OVA^-, and antigen-positive (Gn^+ or Gc^+) B cells were sorted using a MoFlo Astrios EQ Cell Sorter (Beckman Coulter). FACS data were acquired with Summit 6.0 (Beckman Coulter) and analyzed using FlowJo v10.8 (BD Biosciences).

Sorted cells were processed using the 10X Genomics Chromium Next GEM Single Cell V(D)J kit (v1.1, CG000208) according to the manufacturer's protocol to generate barcoded libraries via GEM formation, reverse transcription, and cDNA amplification. Libraries were sequenced on an Illumina platform.

BCR contigs were assembled and aligned to the reference using Cell Ranger (v6.1.1). Only productive contigs and B cells with paired heavy and light chains were retained after quality filtering. Germline V(D)J gene annotation was performed with IgBlast (v1.17.1), and somatic hypermutations were analyzed using the Change-O toolkit (v1.2.0).

Monoclonal antibody expression and purification

Human antibody heavy- and light-chain genes were synthesized and cloned into respective pCMV3 vectors (pCMV3-CH, pCMV3-CL, or pCMV3-CK). Following transformation into E. coli DH5α (Tsingke, TSC-C01-96) and overnight incubation at 37°C, positive clones were identified by colony PCR and Sanger sequencing, followed by plasmid preparation (CWBIO, CW2105). For protein expression, Expi293F cells were co-transfected with paired plasmids using polyethylenimine (Yeasen, 40816ES03) in 0.9% NaCl. Transfected cultures were maintained under standard growth conditions, with nutrient supplement (OPM Biosciences, F081918-001) added 24 h post-transfection and replenished every 48 h. Supernatants were harvested after 8 days of culture for antibody purification.

Antibodies were purified from clarified supernatant (3,000 × g, 10 min) using Protein A magnetic beads (GenScript, L00695) and a KingFisher system (Thermo Fisher). Final samples were quantified by NanoDrop (Thermo Fisher, 840–317400) and analyzed for purity by SDS-PAGE (LabLead, P42015).

ELISA

Purified SFTSV Gn or Gc proteins (1 μg/mL in Solarbio C1055 buffer) were used to coat ELISA plates overnight at 4°C. After washing and blocking, serially diluted antibodies were added and incubated for 30 min at room temperature. The plates were then incubated with an HRP-conjugated goat anti-human IgG (Jackson ImmunoResearch, 109-035-003; 0.25 μg/mL) for 30 min, followed by tetramethylbenzidine (TMB) substrate (Solarbio, PR1200) for signal development. The reaction was terminated with H_2SO_4, and absorbance at 450 nm was read on a microplate reader (Multiskan Fc, Thermo Scientific).

Surface plasmon resonance

SPR experiments were performed on a Biacore 8K (Cytiva). SFTSV mAbs (human IgG1) were captured by a Sensor Chip Protein A (Cytiva). Various concentrations of SFTSV Gn (His-tag; 1.5625, 6.25, 12.5, 25, and 50 nM) were injected. The response was recorded at room temperature, and the raw data curves were fitted to a 1:1 binding model using Biacore Insight Evaluation Software (Cytiva, v4.0.8).

Pseudovirus neutralization assay

SFTSV Gn/Gc pseudoviruses were produced using a VSV-based system. Briefly, 293T cells were infected with G*ΔG-VSV (Kerafast) and transfected with a plasmid encoding the SFTSV glycoproteins. The culture supernatant containing the pseudoviruses was collected, clarified by filtration, aliquoted, and stored at −80°C. For the neutralization assay, serially diluted monoclonal antibodies were mixed with pseudoviruses and incubated for 1 h at 37°C with 5% CO_2. Huh-7 cells were then added to the mixture. After 48 h, the supernatant was removed, and luminescence was measured following the addition of D-luciferin substrate (PerkinElmer, 6066769) using a microplate reader (PerkinElmer, HH3400). The half-maximal inhibitory concentration (IC_{50}) was determined by fitting the data to a four-parameter logistic model in GraphPad Prism (v9.0.1).

DMS library construction

DMS libraries were constructed as previously described, with modifications for the SFTSV Gn-head domain (residues 20–340). Using the HB29 Gn-head coding sequence as a template, two independent mutant libraries were generated via three rounds of mutagenesis PCR with synthesized primer pools. Each Gn-head variant was constructed with an N-terminal HA tag and a C-terminal MYC tag, linked to a unique 26-nucleotide barcode. Barcode-variant mapping was performed by PacBio sequencing. The mutant libraries were cloned into the pETcon vector and electroporated into DH10B cells for plasmid amplification. Plasmids were then transformed into the EBY100 strain of Saccharomyces cerevisiae as previously reported.[53] Transformed yeast were selected on SD-CAA plates and expanded in SD-CAA liquid medium. Yeast libraries were flash-frozen in liquid nitrogen and stored at −80°C.

High-throughput antibody-escape profiling

Antibody escape mutations were assessed using a FACS-based workflow. Yeast-expressing Gn-head mutants were induced overnight and stained. After incubation with primary Gn mAbs for 30 min at 4°C, cells were stained with secondary antibodies: APC anti-HA.11 (BioLegend, 901524), FITC-conjugated chicken anti-*c*-Myc (icllab, CMYC-45F), and PE-conjugated goat anti-human IgG (Jackson, 109-115-098) for 30 min at 4°C. Double-positive (MYC^+ HA^+) yeast displaying bound mAbs were gated, and mAb-unbound populations adjacent to the main population were sorted and collected. Plasmid DNA was extracted after 40 h of culture, barcodes were PCR-amplified, purified with AMPure XP beads (Beckman Coulter, A63882), and subjected to high-throughput sequencing on an Illumina NovaSeq X Plus platform.

Processing of DMS data

Illumina single-end sequencing reads from Gn-head DMS libraries were processed as described with minor modifications. Raw reads were trimmed to 26 bp and mapped to a barcode-variant dictionary using the dms_variants package (v0.8.9). Variant escape scores were calculated as $F \times (n_{X,ab}/N_{ab})/(n_{X,ref}/N_{ref})$, where $n_{X,ab}$ and $n_{X,ref}$ is the number of reads representing variant X, and N_{ab} and N_{ref} are the total number of valid reads in antibody-selected (ab) and reference (ref) library, respectively. F is a normalization factor defined as the 99th percentile of escape fraction ratios. Variants with fewer than six reads in the reference library or those associated with severely impaired Gn-head expression were excluded. Global epistasis models were fitted using dms_variants to infer per-mutation escape scores. Escape scores were averaged across replicates that passed quality control.

Site-level escape scores were computed as the sum of mutation escape scores per Gn-head residue. These scores were used as antibody-specific features to generate a matrix $A_{N\times M}$, where N is the number of antibodies and M is the number of valid positions. Non-surface residues on Gn-head were removed from the analysis. We calculated the pairwise similarities, defined as the square root of the Jensen-Shannon divergence (scipy, v1.11.2) between the feature vectors of two antibodies. The dissimilarity (1.0 - similarity) matrix were used to build a k-nearest neighbor graph (k = 6) and clustered into epitope groups using Leiden algorithm (leidenalg, v0.10.2) with resolution = 2.5. These clusters are then refined by integrating structural mapping, V(D)J germline usage, and neutralization data to define biologically meaningful epitope groups.

Authentic virus neutralization assay

Neutralizing activity of mAbs against authentic SFTSV was measured using an FRNT. The four representative SFTSV strains used for testing include HBMC16, WCH, HNXY2017-50, and HNXY2017-66.[18] Briefly, serially diluted mAbs were incubated with SFTSV virions for 1 h at 37°C. The mixture was added to Vero cells and incubated for 1.5 h at 37°C. Cells were then cultured for 3.5 days in DMEM containing 1.25% methylcellulose. After fixation with 3.7% paraformaldehyde for 30 min, cells were stained with an anti-SFTSV NP primary antibody, followed by an HRP-conjugated anti-mouse secondary antibody (Applygen, C1308). Staining was developed using a DAB substrate (TIANGEN, PA110). Plaque numbers were recorded, and $FRNT_{50}$ values were calculated.

In vivo SFTSV challenge experiment

Mouse studies were conducted as previously described.[18] To assess the prophylactic efficacy, *IFNAR1*$^{-/-}$ mice received a single intraperitoneal (IP) injection of 5 mg/kg of each mAb or a human IgG1 isotype control antibody one day before IP inoculation with 20 FFUs of SFTSV HBMC16. Mice were monitored daily for clinical signs, body weight, and mortality for over 12 days. Weight data are expressed as percentages of initial weight. Serum samples were collected at 3 days post-infection (dpi) for viral load analysis. The therapeutic assessment was largely identical to the prophylactic experiment described above, except that administration occurred one day post-infection. Serum was collected at 3 and 5 dpi for viral load quantification. At 5 dpi, four mice per group were euthanized, and spleen, lung, and liver samples were harvested for viral load determination.

RT-qPCR assay

Total RNA from tissues was extracted using the RNAprep Pure Cell Kit (TIANGEN, DP430). Intracellular viral RNA was quantified by RT-qPCR targeting the SFTSV L segment with primes: SFTSV-L-F: 5′-CTCACTCATGCCCTCAACGA-3′ and SFTSV-L-R: 5′-GATGAACTCACCAGCCCTGC-3′. For serum samples, RNA was extracted with the TIANamp Virus RNA Kit (TIANGEN, DP315-R), and viral load was quantified using primers targeting the SFTSV S segment: SFTSV-S-F: 5′-AGCCTAATTGGATATGTCAAATTGC-3′ and SFTSV-S-R: 5′-CGGGTGAAGTGGCTGAAGG-3′.

Protein expression and purification for structural analysis

Expression constructs encoding the ectodomains of SFTSV Gn or Gc were transiently transfected into HEK293F cells using polyethylenimine (Polysciences). Culture supernatants were harvested 7 days post-transfection, concentrated, and exchanged into binding buffer (25 mM Tris-HCl, pH 8.0, 200 mM NaCl). Proteins were first purified by Ni-NTA affinity chromatography, followed by size-exclusion chromatography on a Superose 6 Increase column in final buffer (20 mM HEPES, pH 7.2, 150 mM NaCl). The Gn-head domain was expressed and purified similarly. Antibody Fabs were expressed and purified as previously described.[54]

Cryo-EM sample preparation, data collection and model building

For the preparation of the complexes, the purified HB29-Gn-head was mixed with a 1.5-fold molar excess of fab BD70-4003 and BD70-4017, BD70-4008-fab and BD70-4017, BD70-4003, BD70-4008-fab separately, incubated on ice for 40 min and injected onto a Superdex 200 Increase 5/150 column (Cytiva) equilibrated with buffer 1× PBS. SDS-PAGE analysis confirmed the formation of the HB29-Gn-head-3-17, HB29-Gn-head-8-17, HB29-Gn-head-3, HB29-Gn-head-8 complexes in a stoichiometric ratio respectively.

An aliquot of 4 μL protein sample of complex at a protein concentration of 0.5 mg/mL was loaded onto a glow-discharged 300 mesh grid (Quantifoil Au R1.2/1.3). The grids were blotted with a filter paper at 4°C and 100% humidity,[55] and flash-cooled in liquid ethane using a Thermo Fisher Vitrobot Mark IV and screened using a 200 KV Talos Aectica.

Cryo-EM datasets were collected on a 300kV Thermo Fisher Titan Krios G4 electron microscope equipped with a Falcon 4 camera and a selectris X energy filter (GIF: a slit width of 10eV). The micrographs were collected at a calibrated magnification of ×130,000 using the EPU software (Thermo Fisher Scientific), yielding a pixel size of 0.95 Å at object scale. Movies were recorded at an accumulated electron dose of 60e^{-}Å^{-2} s^{-1} on each micrograph that was fractionated into a stack of 40 frames with a defocus range of −1.0 μm to −2.0 μm.

Data processing was performed using cryoSPARC (v4.7.1).[56] The data underwent several steps including Motion Correction, CTF Estimation, Create Templates, Template Picker, Extract from Micrographs, 2D classification, 2D selection for Ab-initio Reconstruction, and subsequent Homogeneous Refinement. To enhance the density around the HB29-Gn-head-Fab region, local refinement was conducted using UCSF ChimeraX (v1.7)[57] and cryoSPARC. Structural modeling and refinement were performed using WinCoot (v0.9.4.1)[52] and Phenix (v1.21.2).[51] Figures were generated using UCSF ChimeraX (v1.7).[58]

QUANTIFICATION AND STATISTICAL ANALYSIS

SPR assays were performed in two biological replicates. Binding data were analyzed with the Biacore Insight Evaluation Software using a 1:1 binding model. Neutralization assays were performed in at least two biological replicates. The half-maximal inhibitory/neutralization concentrations (IC_{50}/$FRNT_{50}$) were derived from curve fitting based on a four-parameter logistic regression model.